Doppler-Free Two-Photon Excitation Spectroscopy and the Zeeman Effects. Perturbations in the 14_0^1 and $1_0^1 14_0^1$ Bands of the $S_1 \leftarrow S_0$ Transition of C_6D_6

Dae Youl Baek, Jinguo Wang, Atsushi Doi, Shunji Kasahara, and Hajime Katô*

Molecular Photoscience Research Center, Kobe University, Nada-ku, Kobe 657-8501, Japan

Masaaki Baba

Department of Chemistry, Graduate School of Science, Kyoto University, Kyoto 606-8501, Japan

Received: March 14, 2005; In Final Form: April 28, 2005

Doppler-free two-photon excitation spectra and the Zeeman effects for the $1_0^1 14_0^1$ band of the $S_1\ ^1B_{2u} \leftarrow S_0\ ^1A_{1g}$ transition in gaseous benzene-d_6 were measured. Although the spectral lines were strongly perturbed, almost all of the lines near the band origin could be assigned. From a deperturbation analysis, the perturbation near the band origin was identified as originating from an anharmonic resonance interaction. Perturbation centered at $K = 28-29$ in the 14_0^1 band was analyzed, and it was identified as originating from a perpendicular Coriolis interaction. The symmetry and the assignment of the perturbing state proposed by Schubert et al. (Schubert, U.; Riedle, E.; Neusser, H. J. *J. Chem. Phys.* **1989**, *90*, 5994.) were confirmed. No perturbation originating from an interaction with a triplet state was observed in both bands. From the Zeeman spectra and the analysis, it is demonstrated that rotationally resolved levels are not mixed with a triplet state. The intersystem mixing is not likely to occur at levels of low excess energy in the S_1 state of an isolated benzene. Nonradiative decay of an isolated benzene in the low vibronic levels of the S_1 state will occur through the internal mixing followed by the rotational and vibrational relaxation in the S_0 state.

Introduction

Benzene is a prototype aromatic molecule, and the dynamics in the excited states has been studied extensively.[1−4] Electronic relaxation from the S_1 state can occur via three pathways: radiative transition to the S_0 state, nonradiative transition to isoenergetic levels of vibrationally highly excited levels of the S_0 state (internal conversion: IC), and the one of a triplet state (intersystem crossing: ISC). The fluorescence quantum yield of the $S_1\ ^1B_{2u}$ state of an isolated benzene was observed to be small, and the electronic nonradiative decay was attributed to ISC.[5−8]

Extremely high-resolution can be achieved by Doppler-free two-photon excitation (DFTPE) spectroscopy, and this technique was successfully applied to benzene more than 20 years ago.[9−11] DFTPE spectra of the $1_0^1 14_0^1$ and 14_0^1 bands of C_6D_6 were measured by Sieber et al.[11] Only a part of the $J = K$ lines were assigned in the $1_0^1 14_0^1$ band, and the rotational structure was reported to be impossible to analyze. Through an analysis of intensity fluctuations, the $1_0^1 14_0^1$ band was reported to be chaotic.[12] The dispersed emission spectra from single rovibronic states after DFTPE were measured by Schubert et al.,[13] and it was concluded that most of the rotational levels in the $1^1 14^1$ state are perturbed by selective coupling to only one dark background state.

We have measured the DFTPE spectra and the Zeeman effects of the $1_0^1 14_0^1$ band of the $S_1\ ^1B_{2u} \leftarrow S_0\ ^1A_{1g}$ transition in gaseous benzene-d_6. Accurate frequency marks and the Zeeman effect greatly facilitated the assignment of the complicated spectrum. The spectral lines of the $1_0^1 14_0^1$ band were found to be strongly perturbed, whereas almost all of the lines near the band origin could be assigned. The results and analysis are reported in section A. A deperturbation analysis for the observed perturbations centered at $K = 28-29$ of the 14_0^1 band of C_6D_6 could be achieved, and the results are reported in section B.

Zeeman spectra combined with high-resolution spectroscopies have proven to be advantageous in the identification of the coupling between singlet and triplet states in carbon disulfide and glyoxal.[14,15] The rotationally resolved spectra and the Zeeman effects of the 6_0^1, $1_0^1 6_0^1$, $1_0^2 6_0^1$, and $1_0^1 14_0^1$ bands of the $S_1 \leftarrow S_0$ transition of C_6H_6 and the 14_0^1 band of C_6D_6 were reported.[16−18] A number of energy shifts of the levels in the S_1 state were observed, and all of the perturbing levels were demonstrated to be a singlet state by the Zeeman effects. We have extended the studies on the Zeeman effects, and the results are reported in section C.

Experimental Section

The experimental scheme for DFTPE spectroscopy using counter-propagating light beams of identical wavelength within an external cavity used in this experiment is similar to that previously reported.[15] An external cavity consisting of two spherical mirrors was used to enhance the radiation field. Two-photon absorption was achieved by using a linearly polarized laser beam. The distance between the spherical front mirror (r = 100 mm) of 90% reflectivity and the spherical end mirror (r = 100 mm) of 99.9% reflectivity mounted on a piezo ring actuator was set to 190 mm, in a near concentric arrangement. Benzene-d_6 (Euriso-top, purity of 99.96%) was purified via freeze melt saw. A small portion of the purified benzene was placed in a sample cell, which was mounted within the cavity. The finesse of the cavity was approximately 45, with which a

* To whom correspondence should be addressed. E-mail: h-kato@kobe-u.ac.jp.

10.1021/jp0513115 CCC: $30.25 © 2005 American Chemical Society
Published on Web 07/27/2005

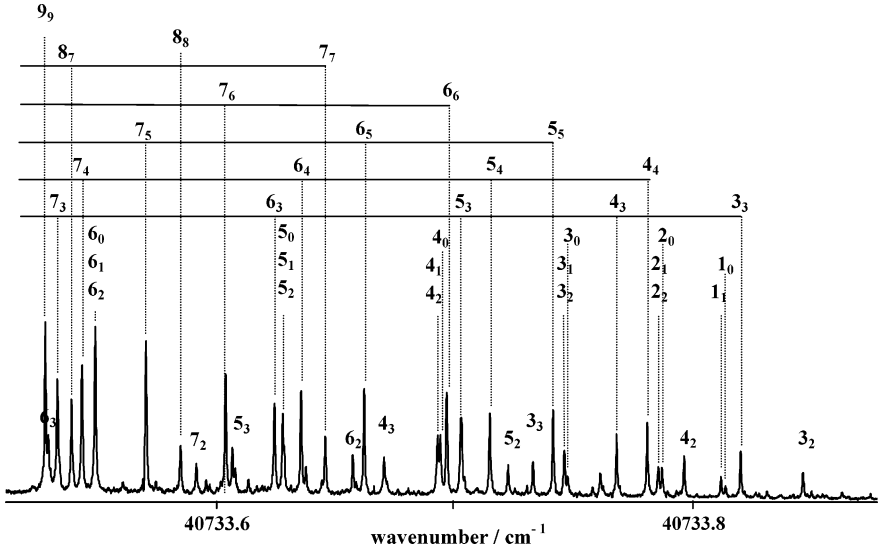

Figure 1. Doppler-free two-photon excitation spectrum around the band origin of the $S_1\ ^1B_{2u}(\nu_1 = 1, \nu_{14} = 1) \leftarrow S_0\ ^1A_{1g}(\nu = 0)$ transition of benzene-d_6. Assignments of the $^{Q(K)}Q(J)$ lines are indicated as J_K above the spectral lines marking with dotted lines, whereas those without dotted lines are transitions to perturbing levels.

radiation power of approximately 11 W could be obtained within the cavity under an input power of 250 mW. A vapor pressure of approximately 1 Torr was maintained in the cell and this resulted in a spectral line width of about 15 MHz caused principally by pressure broadening. Part of the scanning laser beam was phase-modulated at 30 MHz by an electrooptic modulator (New Focus 4001) and was subsequently passed through a stabilized Etalon (Burleigh CFT-500S). This yields fringe marks at every 30 MHz (corresponding to 60 MHz for two-photon absorption) with a finesse of 30. Another portion of the scanning laser beam was taken to record the Doppler-free saturation spectrum of $^{130}Te_2$. Both of the Etalon marks and the saturation spectrum were recorded simultaneously with the DFTPE spectrum.

An electromagnet with conical pole pieces of 60-mm diameter tapered to 15-mm diameter was used for the Zeeman experiments. The magnetic field was applied perpendicular to the propagation vector of the laser beam, whose plane of polarization was perpendicular to the magnetic field (σ pump). The DFTPE spectra at the magnetic fields of $H = 0$, 0.8, and 1.2 T were measured alternatively for a range of 30 GHz with an overlapping of 2 GHz in every adjacent scan. The lines of $^{130}Te_2$ at 19 921.4353, 19 926.5441, 20 362.2786, and 20 365.2275 cm^{-1}, whose wavenumbers were taken from the tellurium atlas,[19] were used to calibrate the spectra by taking into account the +0.0020 cm^{-1} shift.[20] The relative and absolute wavenumbers of the spectral lines can be determined with precisions of ±0.0001 and ±0.001 cm^{-1}, respectively.

Results and Analysis

A. $1_0^1 14_0^1$ Band of C_6D_6. The DFTPE spectrum and the Zeeman effect of the $1_0^1 14_0^1$ band in the $S_1 \leftarrow S_0$ transition of C_6D_6 were measured in the range from 40723.7 to 40734.0 cm^{-1}. The DFTPE spectrum around the band origin is shown in Figure 1. Only $^{Q(K)}Q(J)$ lines are observed, and the assignments are indicated as J_K, where J and K are the quantum numbers of the rotational angular momentum and its projection along the c axis, respectively. The spectrum is strongly perturbed and is difficult to assign at a first glance. It was reported in ref 11 that this band could not be analyzed and only the $J = K$ lines seemed to be in the neighborhood of the expected positions.

We shall describe how these spectral lines were assigned. At first, the DFTPE spectrum was simulated using the molecular constants of the $S_0\ ^1A_{1g}(\nu = 0)$ and $S_1\ ^1B_{2u}(\nu_{14} = 1)$ states reported in refs 21 and 18, respectively. Then, by comparing the simulated spectrum and the observed spectrum of the $1_0^1 14_0^1$ band, a series of $^{Q(K=J)}Q(J)$ lines and the $^{Q(K)}Q(J)$ lines of K close to J were assigned. In this procedure, the Zeeman spectrum was very useful because the Zeeman splittings in the $^{Q(K)}Q(J)$ lines of a given J increased as K increased and those of $^{Q(K=J)}Q(J)$ lines increased linearly with J as it is described in section C. An example is shown in Figure 2: the Zeeman splittings of the 28_{28} and 27_{27} lines are large, whereas the ones of the 20_4, 20_5, 20_6, and so forth are small.

To assign the lines of low J around the band origin, where the Zeeman splittings were small, it was important to find a series of lines with regular energy spacings that could be assigned as J_K lines of $K = 0$, 1, and 2. Then, the perturbation centered at $K = 2-3$ could be found, and a series of transitions to the bright (perturbed) and dark (perturbing) levels were assigned. The assignments are indicated in Figure 1. In this way, we could assign almost all of the lines of appreciable intensity in the range from the band origin to 40 731.4 cm^{-1}.

In the region of 40 723.7−40 731.4 cm^{-1}, some lines with appreciable intensities could not be assigned, and examples of unassigned lines can be seen in Figure 2. Zeeman splittings of some high J and K lines are large and overlapped with neighboring lines at $H = 1.2$ T. In this case, the Zeeman spectra at $H = 0.8$ T are used for the assignment. Totally, 613 lines were assigned, and the data field is shown in Figure 3. Many of unassigned lines were found overlapping with other perturbed lines within the interaction energy, and the assignments without ambiguity were difficult. The perturbations are estimated as originating from interactions with one or two dark vibrational levels because the density of the unassigned lines are compatible with it.

By fixing the molecular constants of the ground state to those reported in ref 21, the molecular constants of the $S_1\ ^1B_{2u}(\nu_1 = 1, \nu_{14} = 1; b_{2u})$ state were fitted using a least-squares fitting of the transition energies of assigned 613 lines including the strongly perturbed ones. The molecular constants $B = A = 0.150465(5)$, $C = 0.075265(6)$, and $T_v = 40733.837(2)$ cm^{-1} were determined with the standard deviation 0.0027 cm^{-1}.

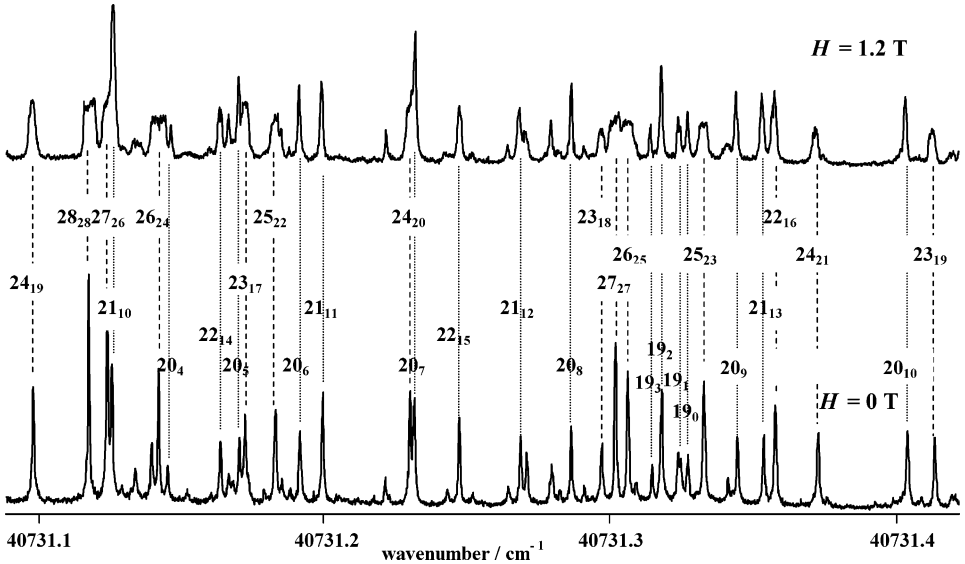

Figure 2. Doppler-free two-photon excitation spectra of the $S_1\ ^1B_{2u}(v_1 = 1, v_{14} = 1) \leftarrow S_0\ ^1A_{1g}(v = 0)$ transition of benzene-d_6 in the regions of 40 731.09−40 731.42 cm^{-1} at the magnetic field $H = 1.2$ T and $H = 0$ T. Assignments of the $^{Q(K)}Q(J)$ lines are indicated as J_K.

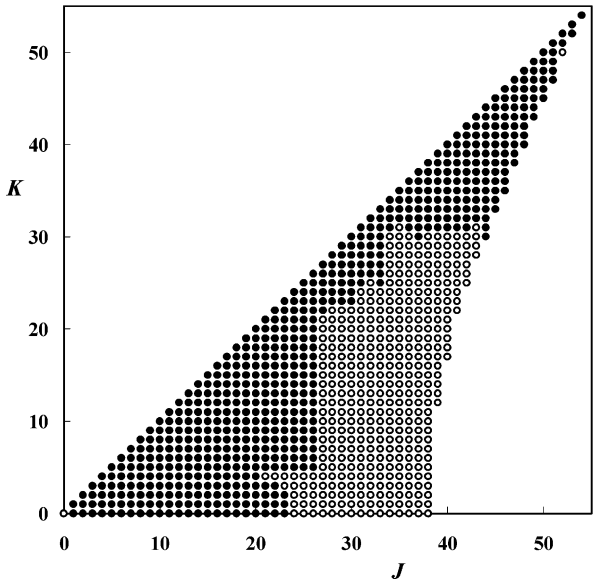

Figure 3. Data field of the $S_1\ ^1B_{2u}(v_1 = 1, v_{14} = 1, J, K) \leftarrow S_0\ ^1A_{1g}(v = 0, J, K)$ transitions of benzene-d_6. Assigned lines are shown by bullets (●). Lines, which are expected to lie within the measured spectra and could not be assigned, are plotted by circles (○).

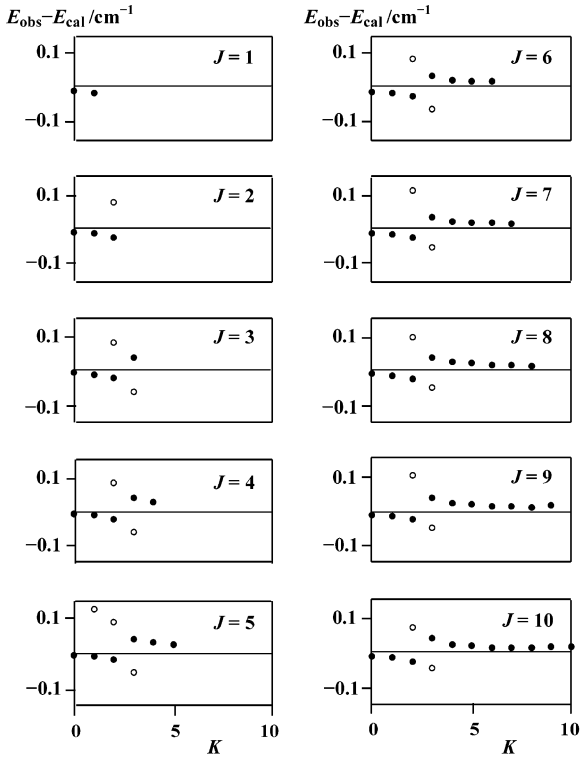

Figure 4. Residuals $E_{obs} - E_{cal}$ of the $S_1\ ^1B_{2u}(v_1 = 1, v_{14} = 1, J, K) \leftarrow S_0\ ^1A_{1g}(v = 0, J, K)$ transitions for $J = 1-10$ are plotted by bullets (●) against K. If two lines of different intensities were observed for a given K, the strong one is marked by a bullet (●) and the weak one by a circle (○).

The difference between the observed transition energy, E_{obs}, and the energy calculated from the molecular constants, E_{cal}, is plotted in Figure 4 against K for rotational levels of $J = 1-10$. Two lines of different intensities for a given K were observed for strongly perturbed levels. The strong and weak components are transitions to the bright and dark levels, respectively, and those are marked on the figure by bullets and circles, respectively. The magnitudes of the Zeeman splittings of the bright and dark levels are almost the same, and hence the electron spin angular momenta of the bright and dark levels are identified to be the same, $S = 0$. Thus, all of the perturbing states in the $1_0^1 14_0^1$ band are confirmed to be a singlet state from the Zeeman spectra. This is consistent with the conclusion derived from the emission spectra by Schubert et al.[13] that the perturbing state is another vibronic state in S_1.

According to the deperturbation analysis for a two-level interaction,[16,22] the energies E_+ and E_- of two levels coupled through an interaction matrix element, V_{bd}, are given by

$$E_{\pm} = \frac{E_b + E_d}{2} \pm \frac{1}{2}[4V_{bd}^2 + (E_b - E_d)^2]^{1/2} \qquad (1)$$

where E_b and E_d are deperturbed energies of bright and dark levels, respectively. From eq 1, we have

$$E_+ + E_- = E_b + E_d \qquad (2)$$

TABLE 1: Observed Energies E_+ and E_- in the $1_0^1 14_0^1$ Band of C_6D_6, the Deperturbed Energy of a Bright Level E_b Calculated from the Molecular Constants, the Deperturbed Energy of a Dark Level $E_d = E_+ + E_- - E_b$, and the Interaction Matrix element $V_{bd} = [-(E_+ - E_b)(E_- - E_b)]^{1/2}$ [a]

J	K	E_+	E_-	E_b	E_d	V_{bd}
5	1	40 733.7612	40 733.6284	40 733.6415	40 733.7481	0.0396
2	2	40 733.8849	40 733.7859	40 733.8069	40 733.8638	0.0405
3	2	40 733.8468	40 733.7463	40 733.7680	40 733.8252	0.0413
4	2	40 733.7964	40 733.6933	40 733.7161	40 733.7736	0.0428
5	2	40 733.7334	40 733.6284	40 733.6512	40 733.7106	0.0433
6	2	40 733.6580	40 733.5491	40 733.5733	40 733.6338	0.0452
7	2	40 733.5917	40 733.4568	40 733.4825	40 733.5661	0.0529
8	2	40 733.4697	40 733.3511	40 733.3786	40 733.4422	0.0500
9	2	40 733.3573	40 733.2326	40 733.2618	40 733.3281	0.0528
10	2	40 733.1960	40 733.0993	40 733.1320	40 733.1632	0.0457
3	3	40 733.8209	40 733.7231	40 733.7842	40 733.7599	0.0474
4	3	40 733.7684	40 733.6714	40 733.7323	40 733.7075	0.0469
5	3	40 733.7032	40 733.6073	40 733.6674	40 733.6432	0.0464
6	3	40 733.6247	40 733.5289	40 733.5895	40 733.5642	0.0462
7	3	40 733.5327	40 733.4471	40 733.4986	40 733.4812	0.0419
8	3	40 733.4287	40 733.3424	40 733.3948	40 733.3763	0.0422
9	3	40 733.3118	40 733.2257	40 733.2780	40 733.2594	0.0420
10	3	40 733.1812	40 733.0953	40 733.1482	40 733.1283	0.0418
					$B_v = 0.15051(7)$	
					$C_v = 0.0591(9)$	
					$T_v = 40733.958(7)$	

[a] B_v, C_v, and T_v are the molecular constants of the dark state. All values are in units of cm^{-1}.

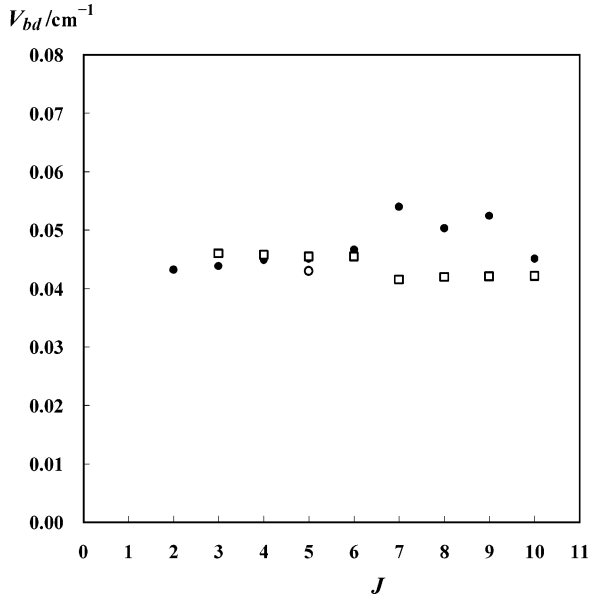

Figure 5. The values of V_{bd} for the S_1 $^1B_{2u}(\upsilon_1 = 1, \upsilon_{14} = 1, J, K)$ levels, which are listed in Table 1, are plotted against J by squares (□) for $K = 0$, bullets (●) for $K = 1$, and circles (○) for $K = 2$.

E_d is calculated by eq 2 using the observed $E_\pm$ values, and E_b is calculated from the molecular constants. Then, the interaction matrix element, V_{bd}, can be calculated by eq 1. The matrix elements, V_{bd}, and the deperturbed energies, E_d, of the dark levels were obtained for the perturbations centered at $K = 1-3$. The results are listed in Table 1, and the values of V_{bd} are plotted against J in Figure 5. The interaction energies, V_{bd}, for the S_1 $^1B_{2u}(\upsilon_1 = 1, \upsilon_{14} = 1, J = 2-10, K = 1-3)$ levels are approximately independent of J and K. Therefore, the observed perturbations are not originating from a Coriolis interaction and may be originating from an anharmonic resonance interaction between two nearby vibrational levels in the S_1 state. The selection rules for an anharmonic resonance interaction are $\Delta J = 0$, $\Delta K = 0$. The molecular constants, B_v, C_v, and T_v, of the perturbing levels were determined by a least-squares fitting to the deperturbed term energies, E_d, and the results are also listed in Table 1.

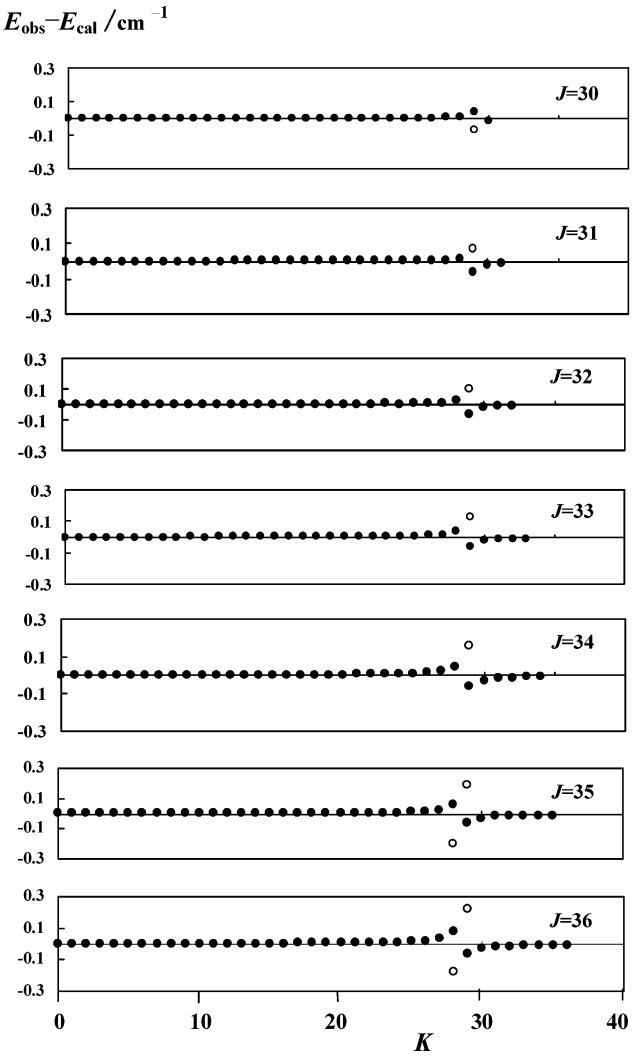

Figure 6. Residuals $E_{obs} - E_{cal}$ of the S_1 $^1B_{2u}(\upsilon_{14} = 1, J, K) \leftarrow S_0$ $^1A_{1g}(\upsilon = 0, J, K)$ transitions for $J = 30$ to 36 are plotted by bullets (●) against K. If two lines of the same (J, K) were observed, then the strong one is marked by a bullet (●) and the weak one by a circle (○).

B. Perturbations in the 14_0^1 Band of C_6D_6. The DFTPE spectrum and the Zeeman effects of the 14_0^1 band of C_6D_6 were studied in ref 18, and the molecular constants of the S_1 $^1B_{2u}$-$(\upsilon_{14} = 1; b_{2u})$ state were reported. To extend this work, we alalyzed the perturbations centered at $K = 28-29$. The differences $(E_{obs} - E_{cal})$ for the rotational levels of $J = 30-36$ in the 14_0^1 band are plotted against K in Figure 6. Two lines of different intensities for a given K were assigned for strongly perturbed levels, and the strong and weak components are marked by bullets and circles, respectively. The interaction energies, V_{bd}, for the S_1 $^1B_{2u}(\upsilon_{14} = 1, J = 30-36, K = 29)$ levels and the deperturbed term energies are calculated in the way described in section A, and the results are listed in Table 2.

The interaction matrix element, V_{bd}, is proportional to K in a parallel Coriolis interaction, while proportional to $[J(J+1) - K(K \pm 1)]^{1/2}$ in a perpendicular Coriolis interaction.[23] The V_{bd} values for the S_1 $^1B_{2u}(\upsilon_{14} = 1, J = 30-36, K = 29)$ levels are observed to increase as J increases (see Table 2 and Figure 7). Therefore, the observed perturbation can be identified as originating from a perpendicular Coriolis interaction. The

TABLE 2: Observed Energies E_+ and E_- in the 14_0^1 Band of C_6D_6, the Deperturbed Energy of a Bright Level E_b Calculated from the Molecular Constants, the Deperturbed Energy of a Dark Level $E_d = E_+ + E_- - E_b$, and the Interaction Matrix Element $V_{bd} = [-(E_+ - E_b)(E_- - E_b)]^{1/2}$ [a]

J	K	E_+	E_-	E_b	E_d	V_{bd}	$\zeta^{Coriolis}$
30	29	39 852.6525	39 852.5442	39 852.6110	39 852.5857	0.0527	0.0049
31	29	39 852.2805	39 852.1461	39 852.2115	39 852.2151	0.0672	0.0050
32	29	39 851.8975	39 851.7347	39 851.7991	39 851.8331	0.0796	0.0051
33	29	39 851.5010	39 851.3101	39 851.3737	39 851.4374	0.0900	0.0051
34	29	39 851.0931	39 850.8727	39 850.9355	39 851.0303	0.0995	0.0051
35	29	39 850.6745	39 850.4221	39 850.4844	39 850.6122	0.1088	0.0051
36	29	39 850.2428	39 849.9585	39 850.0204	39 850.1809	0.1173	0.0052
35	28	39 850.3589	39 850.1049	39 850.2997	39 850.1641	0.1074	0.0048
36	28	39 849.9105	39 849.6570	39 849.8357	39 849.7318	0.1156	0.0048
38	28	39 848.9850	39 848.7179	39 848.8691	39 848.8338	0.1324	0.0049
39	28	39 848.5068	39 848.2282	39 848.3664	39 848.3686	0.1393	0.0049
					$B_v = 0.151003(3)$		
					$C_v = 0.07783(3)$		
					$T_v = 39849.51(2)$		

[a] The Coriolis constant $\zeta^{Coriolis}$ is calculated by $\zeta^{Coriolis} = V_{bd}/[J(J+1) - K(K-1)]^{1/2}$. B_v, C_v, and T_v are the molecular constants of the dark state. All values are in units of cm^{-1}.

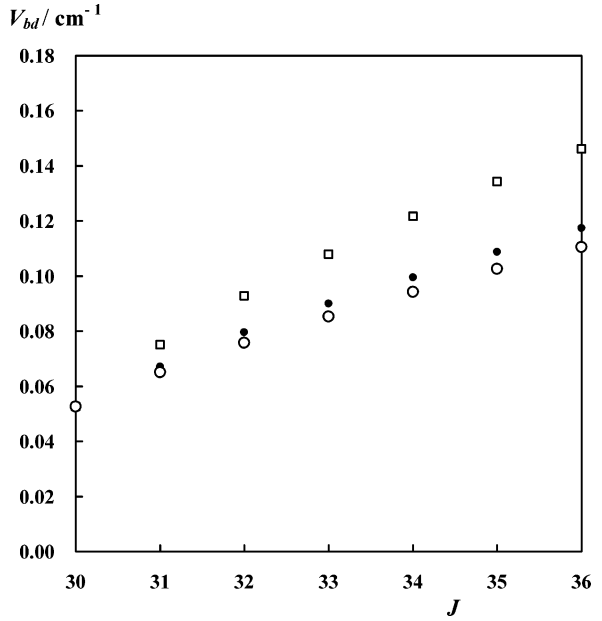

Figure 7. The values of V_{bd} for the $S_1\ ^1B_{2u}(\upsilon_{14} = 1, J, K = 29)$ levels, which are listed in Table 2, are plotted by bullets (●) against J. Values of $\zeta^{Coriolis}[J(J+1) - 29(29+1)]^{1/2}$ and $\zeta^{Coriolis}[J(J+1) - 29(29-1)]^{1/2}$ are plotted against J by squares (□) and circles (○), respectively, where values of $\zeta^{Coriolis}$ were calculated separately for $V_{bd} = 0.0527$ cm^{-1} at $J = 30$.

selection rule for a perpendicular Coriolis interaction is $\Delta J = 0$, $\Delta K = \pm 1$, and the interaction matrix element, V_{bd}, is expressed by

$$V_{bd} = \zeta^{Coriolis}[J(J+1) - K(K \pm 1)]^{1/2} \qquad (3)$$

where $\zeta^{Coriolis}$ is a constant. The $\zeta^{Coriolis}$ constants for the perturbation between the $S_1\ ^1B_{2u}(\upsilon_{14} = 1, J = 30, K = 29)$ level and perturbing levels of $K = 30$ and $K = 28$ are calculated separately for $V_{bd} = 0.0527$ cm^{-1}. For the separately calculated constants, the $\zeta^{Coriolis}[J(J+1) - 29(29+1)]^{1/2}$ and $\zeta^{Coriolis}[J(J+1) - 29(29-1)]^{1/2}$ values are calculated for $J = 30-36$, and those are plotted against J by squares and circles, respectively, in Figure 7. The V_{bd} values obtained by the deperturbation analysis, which are plotted by bullets (●), are close to $\zeta^{Coriolis}[J(J+1) - 29(29-1)]^{1/2}$ as can be seen in Figure 7. Accordingly, the quantum number, K, of the perturbing level is identified to be 28. The $\zeta^{Coriolis}$ constants are calculated by $V_{bd}/[J(J+1) - K(K-1)]^{1/2}$ for each V_{bd} of a given (J, K), and the results are listed in Table 2. The $\zeta^{Coriolis}$ constant is found to be approximately 0.005 cm^{-1} as shown in Table 2. The molecular constants, B_v, C_v, and T_v, of the perturbing levels are determined by a least-squares fitting to the deperturbed energies, E_d, and the results are also listed in Table 2. The $\upsilon_{14} = 1$ level has a b_{2u} symmetry. From the symmetry selection rule for the perpendicular Coriolis interaction (symmetry of the vibrational part of the operator is e_{1g}), the symmetry of the dark vibrational state can be deduced to be e_{2u}. The dispersed emission spectrum from the perturbed $S_1\ ^1B_{2u}(\upsilon_{14} = 1, J = 29, K = 29)$ level was measured by Schubert et al.,[13] and band systems from the bright and dark states were observed. The coupled dark state was assigned as the $4^16^118^1$ state from the coincidence in the level energy with the 14^1 state. The symmetry of the $4^16^118^1$ state is $e_{2u} + a_{1u} + a_{2u}$, and it is consistent with the present assignment to e_{2u} symmetry.

C. Zeeman Spectra. In the preceding paper,[18] it was observed that the Zeeman splittings of the $^{Q(K)}Q(J)$ lines in the 14_0^1 band increased in proportion to K^2 for a given J, and the ones of the $^{Q(K=J)}Q(J)$ lines increased in proportion to J. The magnetic moment of the $S_1\ ^1B_{2u}$ state was found to lie along the c axis (z axis), and the matrix element of the Zeeman interaction, H_Z, for the $S_1\ ^1B_{2u}(\upsilon JKM)$ level was given by

$$\langle S_1\ ^1B_{2u}\upsilon JKM|H_Z|S_1\ ^1B_{2u}\upsilon JKM\rangle = -\frac{MK}{J(J+1)}H\langle S_1\ ^1B_{2u}|m_z|S_1\ ^1B_{2u}\rangle \qquad (4)$$

where the magnetic field, H, is along the space-fixed Z axis, and m_z is the magnetic moment along the molecule-fixed z axis. If the $S_1\ ^1B_{2u}$ state is mixed with the $S_2\ ^1B_{1u}$ state via $J-L$ coupling, the Zeeman splitting of the $^{Q(K)}Q(J)$ line is given by

$$\frac{K^2}{J+1}H\frac{8C_v\langle S_2\ ^1B_{1u}|L_z|S_1\ ^1B_{2u}\rangle}{E(S_2) - E(S_1)}\langle S_1\ ^1B_{2u}|L_z|S_2\ ^1B_{1u}\rangle\mu_B \qquad (5)$$

and the observed Zeeman effects were successfully explained by this model.[18]

In the present study for the $1_0^114_0^1$ band, it is observed that the Zeeman splittings of the $^{Q(K)}Q(J)$ lines of a given J increase in proportion to K^2, and the Zeeman splittings of $K = J$ lines increase in proportion to J as it was observed in the 14_0^1 band. The J dependence of the Zeeman splittings for the $^{Q(K=J)}Q(J)$

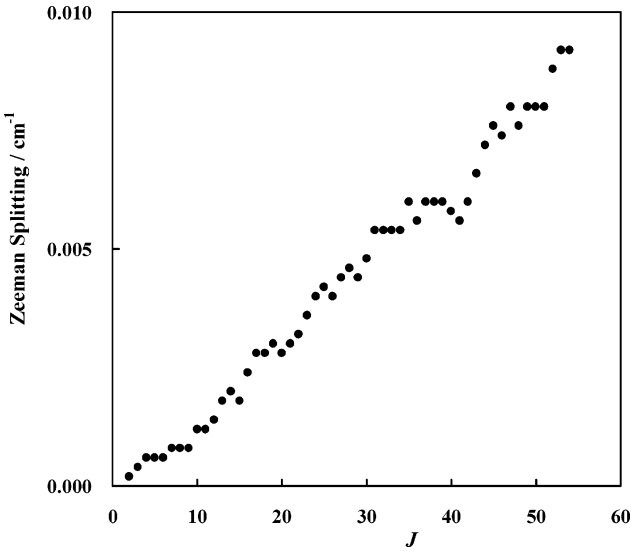

Figure 8. The J dependence of the observed Zeeman splittings of the $^{Q(K=J)}Q(J)$ lines in the $1_0^1 14_0^1$ band of benzene-d_6 at $H = 1.2$ T.

lines is shown in Figure 8. The matrix element $\langle S_2\ ^1B_{1u}|L_z|S_1\ ^1B_{2u}\rangle$ was evaluated to be $-1.729\hbar$ employing simple molecular orbitals.[17] By using the observed values of $E(S_1) = 38290$, $E(S_2) = 46749$ cm^{-1},[24,25] and $C_\upsilon = 0.0753$ cm^{-1}, we calculated the Zeeman splitting of the $S_1\ ^1B_{2u}(\upsilon_1 = 1, \upsilon_{14} = 1, J = 54, K = 54)$ level at $H = 1.2$ T by eq 5 to be 0.0064 cm^{-1}. The observed Zeeman splitting is 0.0092 cm^{-1}, and it is in good accord with the calculated value. The Zeeman splitting is observed to increase in proportion to the magnetic field, H. These are consistent with the conclusion that the Zeeman splitting is originating from the electronic orbital angular momentum arising from a mixing of the $S_1\ ^1B_{2u}$ and $S_2\ ^1B_{1u}$ states via $J-L$ coupling.

The nonradiative decay of benzene excited to low vibrational levels of the S_1 state was attributed to ISC by a number of researchers.[1−4] The primary process for the nonradiative decay was shown to be vibrational rotational mixing in the S_1 state.[13] Let us study this problem. Rotational levels are resolved in the present work, and the molecule is excited to a single eigenstate by a cw single-mode laser. Hence, terminologies such as *internal mixing* and *intersystem mixing* in the stationary state picture are preferred to those such as *internal conversion* and *intersystem crossing* in the time-dependent picture.[26] Unfortunately, the quantum yields of the 14_0^1 and $1_0^1 14_0^1$ bands were not reported to our knowledge. The quantum yields, Q_{fl}, Q_{ISC}, and Q_{IC}, of the 7_0^1 band of C_6D_6 at $E_{excess} = 2320$ cm^{-1}, which is close to the excess energy 2443 cm^{-1} of the $1_0^1 14_0^1$ band, were reported to be 0.17, 0.51, and 0.32, respectively.[27] The ISC was attributed to the $S_1 \rightarrow T_1$ nonradiative transition. If it is, the eigenfunction of the full molecular Hamiltonian of a rotationally resolved excited level $S_1\ ^1B_{2u}(\upsilon JKM)$ is expressed as

$$C^S|JKM> |\upsilon> |S_1\ ^1B_{2u}> + \sum_{m,n} C^T_{m,n}|J_m K_m M_m> |\upsilon_n> |T_1\ ^3B_{1u}> \quad (6)$$

where C^S and $C^T_{m,n}$ are the coefficients. Equation 6 holds even a level in S_1 expressed by $|JKM> |\upsilon> |S_1\ ^1B_{2u}>$ is coupled with many rovibrational levels in T_1 expressed by $|J_m K_m M_m> |\upsilon_n> |T_1\ ^3B_{1u}>$. If the quantum yield of intersystem mixing is 0.5, then the matrix element $\langle S_1\ ^1B_{2u}|m_z|S_1\ ^1B_{2u}\rangle$ in eq 4 can be replaced by $0.5\ \langle T_1\ ^3B_{1u}|m_z|T_1\ ^3B_{1u}\rangle$, and the matrix element of the Zeeman interaction is given by

$$\langle S_1\ ^1B_{2u}\upsilon JKM|H_Z|S_1\ ^1B_{2u}\upsilon JKM\rangle = -\frac{MK}{J(J+1)}H \times 0.5\ \langle T_1\ ^3B_{1u}|m_z|T_1\ ^3B_{1u}\rangle \quad (7)$$

A contribution from an electron spin angular momentum $-g_e S_z \mu_B$ is predominant in the matrix element $\langle T_1\ ^3B_{1u}|m_z|T_1\ ^3B_{1u}\rangle$, where g_e is the g value for an electron, S_z is the z component of an electron spin angular momentum $\boldsymbol{S}$, and μ_B is the Bohr magneton. The matrix element $\langle T_1\ ^3B_{1u}|m_z|T_1\ ^3B_{1u}\rangle$ splits into three components of $M_S = +1, 0, -1$, where the quantum number M_S specifies the projection of the spin angular momentum along the c axis. Therefore, the matrix element $\langle T_1\ ^3B_{1u}| - g_e S_z \mu_B|T_1\ ^3B_{1u}\rangle$ gets values of $-g_e\mu_B$, 0, and $+g_e\mu_B$, respectively. The Zeeman splitting, which is given by the difference of the Zeeman energies of $M = J$ and $M = -J$ components, of the $M_S = \pm 1$ components for the $S_1\ ^1B_{2u}(\upsilon_1 = 1, \upsilon_{14} = 1, J = 54, K = 54)$ level is calculated by eq 7 to be 1.10 cm^{-1} at $H = 1.2$ T. This is larger than the observed Zeeman splitting 0.0092 cm^{-1} by more than 100 times. It is clear from the observed Zeeman spectra that rotationally resolved levels of the S_1 state are not mixed with a triplet state. Therefore, we conclude that nonradiative decay of an isolated benzene molecule excited to the S_1 state does not occur through the intersystem mixing.

Discussion

Compared to the $1_0^1 14_0^1$ band of C_6H_6 at excess energy $E_{excess} = 2492$ cm^{-1}, a drastically reduced number of sharp lines were observed in the $1_0^2 14_0^1$ band of C_6H_6 at $E_{excess} = 3412$ cm^{-1}.[28,29] Lifetimes of single rotational states in the $1^2 14^1$ vibrational state were measured,[30] and the results were coincident with the line width measurement.[11] Coriolis coupling was proposed to be a primary process responsible for the channel three nonradiative process.[29] The onset of the channel three process was reported to be lowered to $E_{excess} = 2400$ cm^{-1} for C_6D_6 as compared to $E_{excess} = 3300$ cm^{-1} for C_6H_6.[27] We found a perpendicular Coriolis interaction in the 14_0^1 band at $E_{excess} = 1568$ cm^{-1} of C_6D_6, and an anharmonic resonance interaction in the $1_0^1 14_0^1$ band at $E_{excess} = 2446$ cm^{-1} of C_6D_6. The $1_0^1 14_0^1$ band of C_6D_6 may lie just below the beginning of the channel three process. In the region of 40 723.7−40 731.4 cm^{-1} of the $1_0^1 14_0^1$ band, the assignments of some lines are difficult. However, the spectral lines are not chaotic, and the line broadening is not observed. The perturbations will be originating from accidental coincidence of level energies of interacting two or three vibrational states.

By a series of studies including the present work,[16−18] it became clear from the Zeeman spectra that rotationally resolved levels in the $S_1(14^1$ and $1^1 14^1)$ states of C_6D_6 and in the $S_1(6^1$, $1^1 6^1$, $1^2 6^1$, and $1^1 14^1)$ states of C_6H_6 are not mixed with a triplet state. From this finding, we conclude that intersystem mixing is not the dominant nonradiative relaxation channel at low excess energy in the S_1 state of benzene. This is at variance with the conclusions of time-resolved measurements and quantum yield measurements.

Isolated benzene in a supersonic molecular beam was excited to a singlet vibronic state by a pulsed frequency-doubled dye laser, and the decay was measured by time-resolved multiphoton ionization mass spectrometry.[31,32] The decay curve was biexponential, and it was analyzed by assuming that the fast component and the slow component were ascribed, respectively,

to the singlet and triplet state decay rates of the initially populated level. However, both components might be ascribed to two vibrational levels of short and long lifetimes in a singlet state because many lines were excited simultaneously. The quantum yields of fluorescence at excess energy 2000 cm^{-1} in the S_1 state were reported to be about 0.20 for C_6H_6 and 0.25 for C_6D_6.[33,34] If the intersystem mixing is not the source of the low quantum yield of fluorescence, the internal mixing must be dominant. Nonradiative decay of an isolated benzene in the low vibronic levels of the S_1 state will occur through the internal mixing followed by the rotational and vibrational relaxation in the S_0 state. The internal mixing is enhanced via anharmonic and Coriolis interactions in the S_1 state. The onset of channel three in benzene was shown to occur via anharmonic−Coriolis coupling in the S_1 state plus IC to the S_0 state.[35] By using a two-photon ionization pump−probe technique with a UV femtosecond pulse, the lifetimes of the vibronic levels at high excess energies in the S_1 state were measured,[36] and the values were found in line with high-resolution measurements.[11] Nonradiative lifetimes in the low vibronic levels in the S_1 state were 10^{-8}−10^{-7} s,[5,33,34,37] and lines broader than our experimental resolution (lifetime shorter than 10^{-8} s) have not been observed for all of the rotationally resolved lines.

In conclusion, it is demonstrated on the basis of the Zeeman spectra and the analysis that rotationally resolved levels are not mixed with a triplet state. Accordingly, it has become clear that the intersystem mixing does not occur at levels of low excess energy in the S_1 state of an isolated benzene. Nonradiative decay in the low vibronic levels of the S_1 state occurs through the internal mixing followed by the rotational and vibrational relaxation in the S_0.

Acknowledgment. This work is supported by a Grant-in-Aid of JSPS and a JSPS research grant for the Future Program: Photoscience.

References and Notes

(1) Parmenter, C. S. *Adv. Chem. Phys.* **1972**, *22*, 365.
(2) Avouris, P.; Gelbart, W. M.; El-Sayed, M. A. *Chem. Rev.* **1977**, *77*, 793.
(3) Ziegler, L. D.; Hudson, B. S. *Excited States* **1982**, *5*, 41.
(4) Lim, E. C. *Adv. Photochem.* **1997**, *23*, 165.
(5) Selinger, B. K.; Ware, W. R. *J. Chem. Phys.* **1970**, *53*, 3160.
(6) Parmenter, C. S.; Schuyler, M. W. *Chem. Phys. Lett.* **1970**, *6*, 339.
(7) Ware, W. R.; Selinger, B. K.; Parmenter, C. S.; Schuyler, M. W. *Chem. Phys. Lett.* **1970**, *6*, 342.
(8) Gelbart, W. M.; Spears, K. G.; Freed, K. F.; Jortner, J.; Rice, S. A. *Chem. Phys. Lett.* **1970**, *6*, 345.
(9) Riedle, E.; Neusser, H. J.; Schlag, E. W. *J. Chem. Phys.* **1981**, *75*, 4231.
(10) Riedle, E.; Stepp, H.; Neusser, H. J. *Chem. Phys. Lett.* **1984**, *110*, 452.
(11) Sieber, H.; Riedle, E.; Neusser, H. J. *J. Chem. Phys.* **1988**, *89*, 4620.
(12) Engel, Y. M.; Levine, R. D. *J. Chem. Phys.* **1988**, *89*, 4633.
(13) Schubert, U.; Riedle, E.; Neusser, H. J. *J. Chem. Phys.* **1989**, *90*, 5994.
(14) Katô, H.; Doi, A.; Taroura, Y.; Nagakura, S. *J. Chem. Phys.* **1995**, *103*, 4869.
(15) Katô, H.; Oonishi, T.; Nishizawa, K.; Kasahara, S.; Baba, M. *J. Chem. Phys.* **1997**, *106*, 8392.
(16) Misono, M.; Wang, J.; Ushino, M.; Okubo, M.; Katô, H.; Baba, M.; Nagakura, S. *J. Chem. Phys.* **2002**, *116*, 162.
(17) Doi, A.; Kasahara, S.; Katô, H.; Baba, M. *J. Chem. Phys.* **2004**, *120*, 6439.
(18) Wang, J.; Doi, A.; Kasahara, S.; Katô, H.; Baba, M. *J. Chem. Phys.* **2004**, *121*, 9188.
(19) Cariou, J.; Luc, P. *Atlas du Spectre d'Absorption de la Molécule de Tellure. Partie 2: 18 500−21 200 cm*$^{-1}$; CNRS: Paris, 1980.
(20) Gillaspy, J. D.; Sansonetti, C. J. *J. Opt. Soc. Am.* **1991**, *B8*, 2414.
(21) Doi, A.; Baba, M.; Kasahara, S.; Katô, H. *J. Mol. Spectrosc.* **2004**, *227*, 180.
(22) Schubert, U.; Riedle, E.; Neusser, H. J.; Schlag, E. W. *Isr. J. Chem.* **1990**, *30*, 197.
(23) Mills, I. M. *Pure Appl. Chem.* **1965**, *11*, 325.
(24) Garforth, F. M.; Ingold, C. K.; Poole, H. G. *J. Chem. Soc.* **1948**, 508.
(25) Pantos, E.; Taleb, A. M.; Hamilton, T. D. S.; Munro, I. H. *Mol. Phys.* **1974**, *28*, 1139.
(26) Henry, B. R.; Kasha, M. *Annu. Rev. Phys. Chem.* **1968**, *19*, 161.
(27) Knee, J. L.; Otis, C. E.; Johnson, P. M. *J. Chem. Phys.* **1984**, *81*, 4455.
(28) Riedle, E.; Neusser, H. J.; Schlag, E. W. *J. Phys. Chem.* **1982**, *86*, 4847.
(29) Riedle, E.; Neusser, H. J. *J. Chem. Phys.* **1984**, *80*, 4686.
(30) Schubert, U.; Riedle, E.; Neusser, H. J.; Schlag, E. W. *J. Chem. Phys.* **1986**, *84*, 6182.
(31) Duncan, M. A.; Dietz, T. G.; Liverman, M. G.; Smalley, R. E. *J. Phys. Chem.* **1981**, *85*, 7.
(32) Otis, C. E.; Knee, J. L.; Johnson, P. M. *J. Phys. Chem.* **1983**, *87*, 2232.
(33) Spears, K. G.; Rice, S. A. *J. Chem. Phys.* **1971**, *55*, 5561.
(34) Abramson, A. S.; Spears, K. G.; Rice, S. A. *J. Chem. Phys.* **1972**, *56*, 2291.
(35) Helman, A.; Marcus, R. A. *J. Chem. Phys.* **1993**, *99*, 5011.
(36) Clara, M.; Hellerer, T.; Neusser, H. J. *Appl. Phys. B* **2000**, *71*, 431.
(37) Wunsch, L.; Neusser, H. J.; Schlag, E. W. *Chem. Phys. Lett.* **1975**, *32*, 210.